High-Performance Ferroelectric–Dielectric Multilayered Thin Films for Energy Storage Capacitors

José P. B. Silva, João M. B. Silva, Marcelo J. S. Oliveira, Tobias Weingärtner, Koppole C. Sekhar,* Mário Pereira, and Maria J. M. Gomes*

Herein, the effect of the insertion of a thin dielectric HfO_2:Al_2O_3 (HAO) layer at different positions in the Pt/0.5Ba($Zr_{0.2}Ti_{0.8}$)O_3–0.5($Ba_{0.7}Ca_{0.3}$)TiO_3 (BCZT)/Au structure on the energy storage performance of the capacitors is investigated. A high storage performance is achieved through the insertion of a HAO layer between BCZT and Au layers. The insertion of the dielectric layer causes a depolarization field which results in a high linearity hysteresis loop with low energy dissipation. The Pt/BCZT/HAO/Au capacitors show an impressive energy storage density of 99.8 J cm^{-3} and efficiency of 71.0%, at an applied electric field of 750 kV cm^{-1}. Further, no significant change in the energy storage properties is observed after passing 10^8 switching cycles through the capacitor. The presence of resistive switching (RS) in leakage current characteristics confirms the strong charge coupling between ferroelectric and insulator layers. The same trend of the RS ratio and the energy storage performance with the variation of the architecture of the devices suggests that the energy storage properties can be improved through the charge coupling between the layers. By combining ferroelectrics and dielectrics into one single structure, the proposed strategy provides an efficient way for developing highly efficient energy storage capacitors.

Dr. J. P. B. Silva, J. M. B. Silva, M. J. S. Oliveira, Prof. M. Pereira, Prof. M. J. M. Gomes
Centro de Física das Universidades do Minho e do Porto (CF-UM-UP)
Campus de Gualtar, 4710-057 Braga, Portugal
E-mail: josesilva@fisica.uminho.pt
Dr. J. P. B. Silva
IFIMUP and IN-Institute of Nanoscience and Nanotechnology
Departamento de Física e Astronomia
Faculdade de Ciências da
Universidade do Porto
Rua do Campo Alegre 687, 4169-007 Porto, Portugal
T. Weingärtner
Institute for Applied Materials–Applied Materials Physics (IAM–AWP)
Karlsruhe Institute of Technology
Kaiserstraße 12, 76131 Karlsruhe, Germany
Dr. K. C. Sekhar
Department of Physics
School of Basic and Applied Sciences
Central University of Tamil Nadu
Thiruvarur 610 101, Tamil Nadu, India
E-mail: koppolechandrasekhar@cutn.ac.in

1. Introduction

Recently, there has been a great demand for high energy storage and conversion devices to meet the exponential growth of power requirement in the modern society.[1,2] Among the various available electrical energy storage devices, such as batteries, supercapacitors, and dielectric capacitors, the dielectric capacitors exhibit unique advantages such as ultrafast charge–discharge speed and high energy storage density.[3,4] Furthermore, the dielectric capacitors are classified as linear dielectric capacitors, antiferroelectric ones and ferroelectric ones based on their polarization behavior.[5] Among them, the ferroelectric film capacitors usually possess short charge–discharge time (in the ns range), that make them suitable candidates for fast energy storage applications.[6]

The energy storage density and the energy storage efficiency are the two key factors that evaluate the performance of the energy storage capacitors. The energy storage density (W_{rev}) of ferroelectric thin film capacitors can be calculated by the integration of the P–E loops, as follows[5,7]

$$W_{rev} = \int_{P_r}^{P_{max}} E \, dP \tag{1}$$

where P_{max} is the maximum polarization and P_r is the remnant polarization. Based on the equation, the high energy storage materials required the features of high P_{max} and low P_r and the large breakdown strength field. On the other hand, the energy storage efficiency (η) can be calculated by using the following equation[5,7]

$$\eta = \frac{W_{rev}}{W_{rev} + W_{loss}} \tag{2}$$

where W_{loss} is the energy dissipated, which mainly depends on the hysteretic depolarization process.

Previously, ferroelectric materials in form of bulk have been investigated as energy storage capacitors, but their practical applications were limited due to high voltages. This high voltage

problem can be overcome with the ferroelectric thin films, but they are limited by low storage capacities.[8] Therefore, different approaches have been employed to improve the energy storage properties, such as doping effect, interface engineering, and stress engineering. For instance, $BiFeO_3$ thin films have shown an energy storage density of 3.2 J cm^{-3} that can be enhanced up to 65.5 J cm^{-3} in a multilayered $BiFeO_3/Bi_{3.25}La_{0.75}Ti_3O_{12}/BiFeO_3$ structure with an efficiency of 74%.[9] An high efficiency of ≈81% with $W_{rev} \approx 37$ J cm^{-3} has been achieved in $0.88BaTiO_3$–$0.12Bi(Mg,Ti)O_3$ films.[10] Moreover, McMillen et al. showed that an insertion of 6 nm alumina on 400 nm of $(BiFeO_3)_{0.6}$–$(SrTiO_3)_{0.4}$ thin film increases recoverable energy of the system by around 30%.[11] More recently, Zhang et al. showed that $PbZr_{0.52}Ti_{0.48}O_3/Al_2O_3/PbZr_{0.52}Ti_{0.48}O_3$ structures exhibit outstanding energy storage density of 63.7 J cm^{-3} and efficiency of 81.3%.[12] However, the presence of toxic or volatile elements such as Pb and Bi is the main drawback in the above structures.

Recently, among various lead-free materials, $Ba_{0.7}Ca_{0.3}TiO_3$-$BaZr_{0.2}Ti_{0.8}O_3$ (BCZT) compound has been receiving wide attention since 2009 due to its large piezoelectric coefficient of ≈620 pC/N and high permittivity resulting from phase coexistence at the morphotropic phase boundary similar to $PbZr_{0.52}Ti_{0.48}O_3$ (PZT).[13] Furthermore, it is known that BCZT thin films show high spontaneous polarization ($Ps \approx 150$ μC cm^{-2})[14] with ultrafast switching speed in the nanoseconds regime[15] that makes them appropriate for the energy storage application. Therefore, BCZT ceramics have been investigated for energy storage applications[16] and an energy storage density of 39.11 J cm^{-3} with an efficiency of 33% was achieved in BCZT thin films.[14] Furthermore, lead-free BCZT/poly(vinylidene fluoride) (PVDF) composites have shown an energy storage density below 10 J cm^{-3} and an efficiency higher than 50%.[17] However, these values are still inferior when compared with those obtained from lead-based materials.

In this work, the strategy adopted was to improve the ferroelectric polarization of BCZT film through its crystalline orientation since (*111*) oriented films usually exhibit high P_{max}–P_r values.[18] Moreover, the integration of BCZT thin films with a thin HfO_2:Al_2O_3 (HAO) dielectric layer, so-called ferroelectric–dielectric structure, modifies the dielectric and ferroelectric behaviors and thus consequently enhances the energy storage performance. Additionally, this work provides an innovative way, where high storage efficiency capacitors can be achieved through the selection of proper architecture of the device. The energy storage efficiency is explained based on the texture of ferroelectric layer, the interface quality, and the charge coupling between ferroelectric–dielectric layers.

2. Results and Discussion

Figure 1 shows the grazing incidence x-ray diffraction (GIXRD) patterns of different architecture composed by BCZT and HAO. The patterns exhibit the characteristic Bragg peaks of the perovskite tetragonal phase of BCZT,[19] without any secondary phase. The films exhibit (*111*)-preferred orientation because the (*111*)-reflection intensities are higher than the other reflections of the perovskite; This orientation may be induced by the

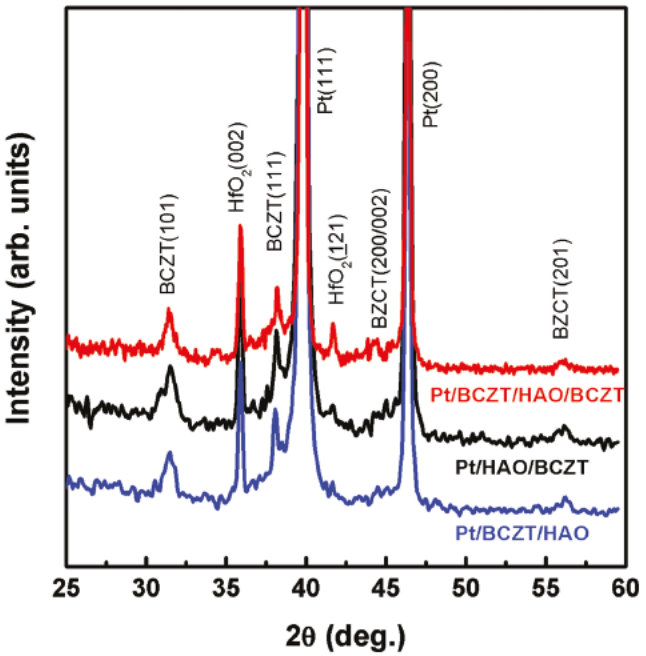

Figure 1. GIXRD patterns of the samples with different architectures based on BCZT and HAO layers.

Pt(*111*)/Ti/SiO_2/Si substrate that acts as a growth template. A qualitative analysis of the films orientation was done by using the following equation[20]

$$\frac{I'}{I'_{101} + I'_{111}} \tag{3}$$

where I' is equal to I/I^*. Here, I and I^* are the intensities of a particular reflection of BCZT as film and as powdered polycrystal, respectively. From the calculated intensity ratio for all the structures, shown in **Table 1**, one can observe that the BCZT layers have the (*111*) preferred orientation. Moreover, it can be seen that the BCZT exhibits a highly (*111*) preferred orientation when it is deposited directly onto the Pt layer. Besides the BCZT peaks, the GIXRD patterns also show the characteristic Bragg peaks of the monoclinic phase of HfO_2 at $2\theta \approx 35.8°$ and 41.7° corresponding to the HfO_2 (*002*) and HfO_2 ($\bar{1}21$) reflections, respectively.[21] It should be pointed out that no Al_2O_3 diffraction peaks were observed suggesting its amorphous nature.

The interfacial chemical sharpness was investigated by Auger electron spectroscopy (AES). **Figure 2**a–c shows the AES

Table 1. Relative intensity ratio of peaks in BCZT layers in different structures.

Structure	$\frac{I'_{101}}{I'_{101}+I'_{111}}$	$\frac{I'_{111}}{I'_{101}+I'_{111}}$
Pt/BCZT/HAO	0.19	0.81
Pt/HAO/BCZT	0.26	0.74
Pt/BCZT/HAO/BCZT	0.30	0.70

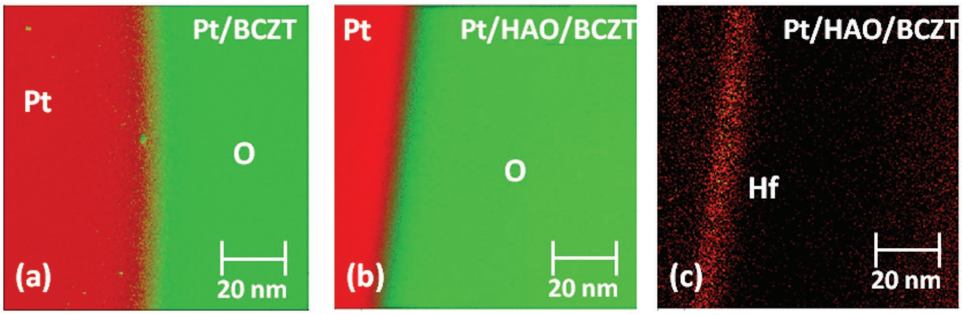

Figure 2. AES maps for the a) Pt/BCZT and b,c) Pt/HAO/BCZT structures. Combined AES color map was obtained by overlapping the Pt and O maps.

maps disclosing the spatial distribution of platinum (Pt) element from the bottom electrode, oxygen (O) element from the BCZT and/or HAO layers, and the hafnium (Hf) element from the HAO layer. The chemical maps clearly demonstrate that the diffusion between the Pt and O elements is more significant for the Pt/BCZT structure (Figure 2a), while the insertion of a HAO layer between the Pt and BCZT layers significantly improves the interface sharpness in the Pt/HAO/BCZT structures, as evidenced in the Figure 2b. In Figure 2c is shown the spatial distribution of the Hf element at the Pt/HAO/BCZT interface to confirm the sharpness of the HAO layer and its thickness (10 nm).

Figure 3 depicts the polarization versus electric field (*P–E*) hysteresis loops for all the capacitors. For comparison, the *P–E* loop of the Pt/BCZT/Au capacitor is also given. The presence of the *P–E* loop confirms that all the structures exhibit a ferroelectric nature. From Figure 3, it is also observed that the shape of the hysteresis is strongly dependent on the architecture of the sample: With the insertion of a dielectric layer, the hysteresis loops become slim and slant; this is beneficial for obtaining high energy storage efficiency due to the smaller hysteresis loss. In fact, the insertion of a dielectric layer can cause a depolarization field, which opposes to the applied electric field, and results in a slanted *P–E* hysteresis loop. The depolarization field can be expressed as follows[22]

$$E_{de} = \frac{P_f d}{\varepsilon_0 (\varepsilon_d L + \varepsilon_f d)} \quad (4)$$

where P_f is the polarization of the ferroelectrics, L and d are the thicknesses of the ferroelectric film and the dielectric thin layer, and ε_0, ε_f, and ε_d are the permittivity of free space, the ferroelectric layer, and the dielectric layer, respectively.

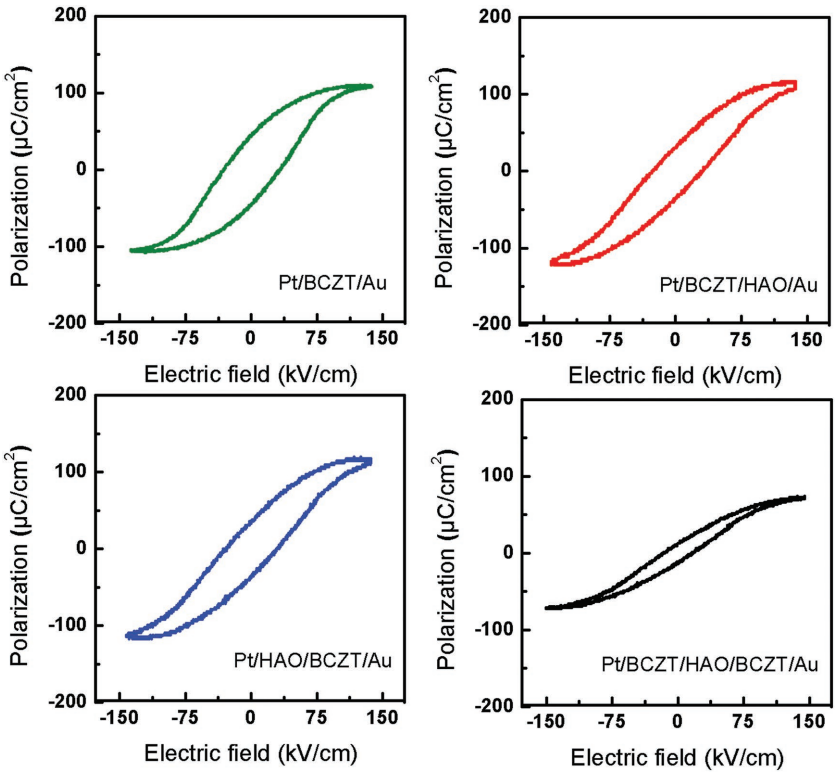

Figure 3. *P–E* hysteresis loops for different architecture of the capacitors.

The average values of average remnant polarization (P_r), maximum polarization (P_{max}), and coercive field (E_c) observed in the capacitors are presented in **Table 2**. It was previously reported that polycrystalline BCZT thin films can exhibit a *Pr* of 37 μC cm^{-2}[23] and a *Ps* of ≈100 μC cm^{-2},[24] while epitaxial BCZT films can exhibit a maximum polarization of 148 μC cm^{-2} and a *Pr* of 95.80 μC cm^{-2}.[14] It is well established that polarization of ferroelectric thin films depended on the texture of the thin films. Usually, the epitaxial films or single crystals exhibit higher polarization than polycrystalline films since there are no grain boundaries to obstruct the domain orientations.[25] Therefore, the observed value of *Pr* ≈ 47 μC cm^{-2} in present BCZT films is quite reasonable and can be attributed due to (*111*) preferred orientation.

From Table 2, it is possible to observe that the insertion of the HAO in different positions strongly influences t he P_r, P_{max}, a nd E_c values. Moreover, the slight increase of P_r and P_{max} values in the Pt/BCZT/HAO/Au capacitor as compared with the ones from the Pt/HAO/BCZT/Au capacitors might be

Table 2. Average remnant polarization (P_r), maximum polarization (P_{max}), and coercive field (E_c) for the different capacitors.

Capacitors	*Pr* [μC cm^{-2}]	P_{max} [μC cm^{-2}]	E_c [kV cm^{-1}]	W_{rev} [J cm^{-3}]	η(%)
Pt/BCZT/Au	47.0	106.5	32.0	2.3	28.5
Pt/BCZT/HAO/Au	37.5	116.5	29.5	3.3	35.9
Pt/HAO/BCZT/Au	33.0	114.5	28.0	3.7	37.5
Pt/BCZT/HAO/BCZT/Au	11.8	71.5	17.0	2.8	60.5

attributed to the highly (*111*)-oriented texture of BCZT films, as evidenced by the GIXRD measurements. The high textured films usually have less grain boundaries and this might facilitate the domain wall motion and thus the polarization is enhanced. Furthermore, the insertion of the HAO layer between the ferroelectric layer and the top/bottom electrode can enhance the quality of the interface, by reducing the thickness of the interfacial passive layer and/or inter diffusion at the interface, as evidenced by the AES analysis, which suppresses the domain wall pinning and thus enhances the polarization.[26] In the case of the Pt/BCZT/HAO/BCZT/Au capacitors, the values of P_r, P_{max}, and E_c decrease significantly. This might be attributed to the fact that each BCZT layer behaves like an individual one with half of the thickness of the other layers. Moreover, it is known that the values of P_r, P_{max}, and E_c are decreasing functions of the ferroelectric layer in Pt/BCZT/HAO/Au capacitors.[26]

Table 2 depicts the calculated values of energy storage density and the energy storage efficiency for all the capacitors, at an applied electric field of ≈150 kV cm^{-1}, besides the ferroelectric polarization values and coercive fields. One can observe that irrespective of the position of the dielectric layer, the capacitors based on BCZT-HAO structures show a superior performance when compared to capacitors based on BCZT. Particularly, Pt/BCZT/HAO/Au capacitors show a 30% enhancement of the recoverable energy density when compared to Pt/BCZT/Au capacitors. This is consistent with the work of M. McMillen et al. that shows that the enhancement in recoverable energy with the insertion of 6 nm alumina layer on $(BiFeO_3)_{0.6}$–$(SrTiO_3)_{0.4}$ ferroelectric capacitors leads to the same amount of enhancement in recoverable energy.[11]

The frequency dependence of the dielectric permittivity and losses of the different capacitors have been studied and are shown in **Figure 4**. The values of dielectric permittivity of the Pt/BCZT/Au, Pt/BCZT/HAO/Au, Pt/HAO/BCZT/Au, and Pt/BCZT/HAO/BCZT/Au are found to be 2347, 764, 627, and 601, at a frequency of 1 kHz, respectively. The dielectric permittivity of the Pt/BCZT/Au capacitor is higher than the one found on literature for polycrystalline thin films[27] and lower than the one from epitaxial BCZT thin films.[28] Moreover, the drastic decrease observed in the dielectric permittivity with the insertion of the dielectric layer agrees well with predictions for a series connection between the ferroelectric and the dielectric layer. From Figure 4, one can observe that the dielectric permittivity decreases with the increase of frequency and this is attributed to the slowdown of the polarization at high frequencies.[17] On the other hand, the dielectric loss values of all the structures show only slight changes over the frequency ranging from 100 Hz to 10 kHz and then increase to the maximum value.

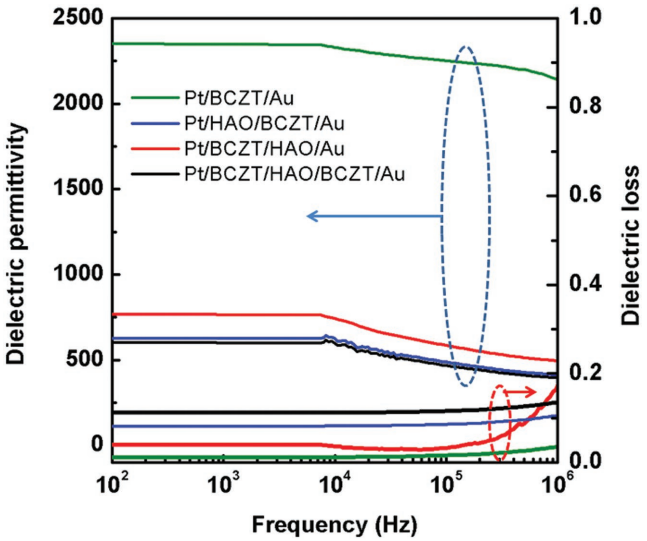

Figure 4. Frequency dependence of dielectric permittivity and losses for all the capacitors.

In order to explain the mechanism of the energy storage density of the different capacitors more clearly, we have measured the leakage current versus voltage (*I*–*V*) for the ferroelectric–dielectric capacitors. The DC voltage V was applied on the bottom Pt electrode with the Au electrode acting as the ground. The *I*–*V* curves for the Pt/BCZT/HAO/Au, the Pt/BCZT/HAO/BCZT/Au, and the Pt/HAO/BCZT/Au capacitors are shown in **Figure 5**. These curves for the different capacitors show the bipolar resistive switching (RS), with two conductive states,

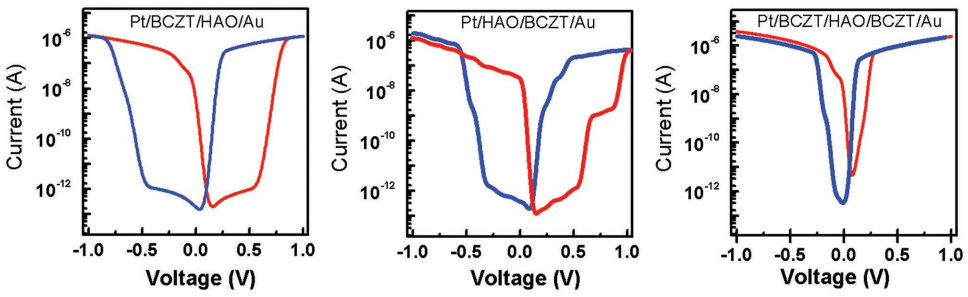

Figure 5. *I*–*V* characteristic curves for all the capacitors.

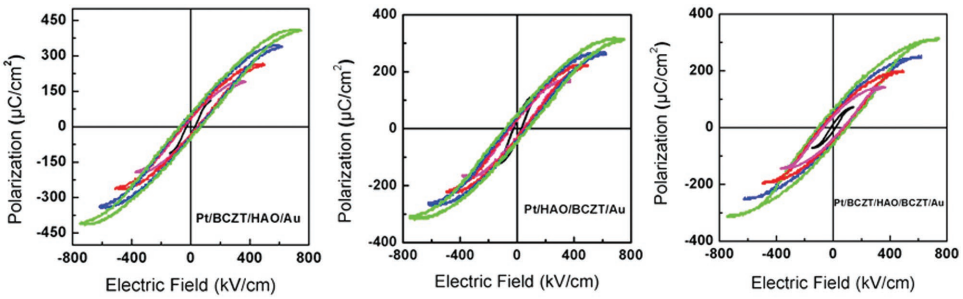

Figure 6. Electrical field dependent *P–E* hysteresis loops for all the capacitors.

known as high resistance state (HRS) and low resistance state (LRS), clearly defined. The diode behavior and the RS effect are attributed to the barrier variation at the BCZT/HAO interface caused by the ferroelectric polarization flipping, as we have shown previously in Pt/BCZT/HAO/Au capacitors.[26] Moreover, the RS ratio (R_{HRS}/R_{LRS}) was found to be ≈10^6, 10^5, and ≈10^4 for the Pt/BCZT/HAO/Au, the Pt/HAO/BCZT/Au, and the Pt/BCZT/HAO/BCZT/Au capacitors, respectively. The decrease on the RS ratio is explained by the decrease of the P_r values. Additionally, the switching field (E_s) was found to be 34.4, 28.5, and 12.5 kV cm^{-1} for the Pt/BCZT/HAO/Au, the Pt/HAO/BCZT/Au, and the Pt/BCZT/HAO/BCZT/Au capacitors, respectively, which is similar to the coercive field obtained from the *P–E* loops for each capacitor. This also confirms that the RS effect is due to the electrostatic coupling between the HAO and the BCZT layers.[20]

Since the energy storage density is strongly dependent on the applied field, the capacitors Pt/BCZT/HAO/Au, Pt/HAO/BCZT/Au, and Pt/BCZT/HAO/BCZT/Au have been chosen to be investigated at high electrical fields. **Figure 6** shows the electric field dependent *P–E* hysteresis loops for these capacitors and **Figure 7**a,b shows a quantitative analysis of the *P–E* loops by evidencing the variation of the average P_r, P_{max}, E_c, and $P_{max} - P_r$ values with the electric field. One can observe that the values of P_r, P_{max}, and E_c tend to increase with the applied electric field. However, it is possible to observe that the $P_{max} - P_r$ values increase more notably with the electric field for the Pt/BCZT/HAO/Au capacitors. This is due to the fact that the P_{max} value increases 72.6%, while P_r softly increases 31.8% in the studied electric field range. Therefore, a higher P_{max}–P_r value leads to a higher linear hysteresis loop, which is obtained for the Pt/BCZT/HAO/Au capacitors.

The energy storage density and the energy storage efficiency were calculated and are presented in **Figure 8**, as a function of the applied electric field from ≈150 to 750 kV cm^{-1}. Figure 8 reveals that the energy storage density and the energy storage efficiency are maximum for the Pt/BCZT/HAO/Au capacitor with an energy storage density of 99.8 J cm^{-3} and efficiency of 71.0%, at 750 kV cm^{-1}. The electric breakdown of the present structures is higher than the one reported for BCZT ceramics (160 kV cm^{-1})[16] and is comparable with the ones reported for $BaTiO_3$ (500 kV cm^{-1}) and BCZT (1000 kV cm^{-1}) thin films.[27,29] The high energy storage performance in this capacitor is attributed to the depolarization field and strong charge coupling caused by the insertion of the dielectric layer, to the high polarization values, but also to the higher difference between the maximum and remnant polarization (P_{max}–P_r) values, which results in a high linearity hysteresis loop with low energy dissipation. Moreover, a similar trend of the RS ratio and the energy storage performance is observed in different architecture of the capacitors. The Pt/BCZT/HAO/Au capacitor shows the highest RS ratio and the highest energy storage energy density and efficiency. This confirms that the charge coupling between ferroelectric-insulator layers can improve energy storage efficiency as it modifies the entire band profile at the interface. **Table 3** shows a comparison of the energy storage density and efficiency obtained in this work with the ones presented in the literature for ferroelectric and ferroelectric–dielectric capacitors. The attractive features of the present Pt/BCZT/HAO/Au capacitors are the excellent energy storage density (99.8 J cm^{-3}), and also the high energy storage efficiency (71%) simultaneously, at an applied electric field of 750 kV cm^{-1}.

From practical application viewpoint, the validation of the capacitor stability under continuous cycling is essential. The *P–E* loops were measured up to 10^8 cycles, at room temperature, and the energy storage properties as a function of the number of cycles are shown in **Figure 9**. The energy storage properties of the Pt/BCZT/HAO/Au capacitors show no significant changes after continuous cycling, as shown in Figure 9, suggesting that the present capacitors are

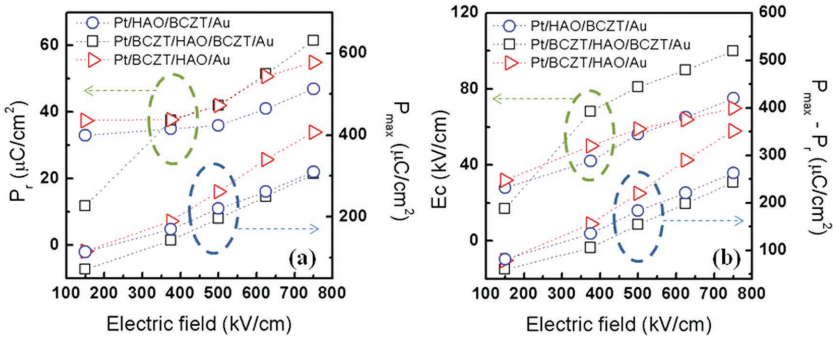

Figure 7. a) P_r and P_{max} and b) E_c and P_{max}–P_r values as a function of the applied electric field.

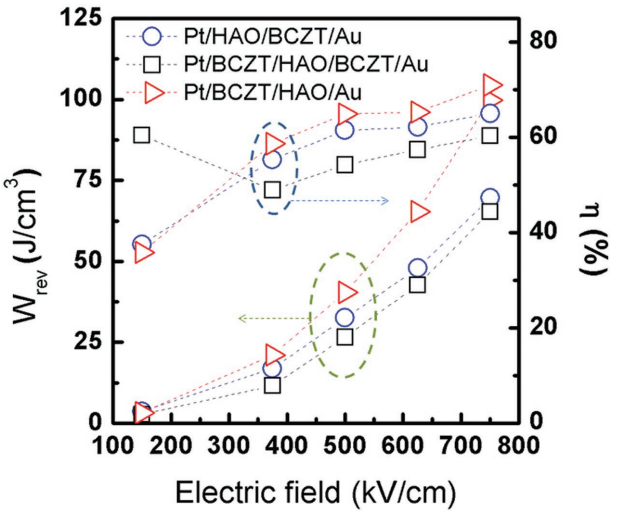

Figure 8. Energy storage density and energy storage efficiency as a function of the applied electric field for the different architecture capacitors.

potential candidates for efficient and ultrafast energy storage applications.

3. Conclusion

In conclusion, the insertion of a thin dielectric HAO layer in a Pt/BCZT/Au capacitor proved to be an innovative strategy to improve the energy storage performance of the capacitors. The insertion of the HAO layer provided a depolarizing field, which counteracts the external electric field, and led to the slimming of the *P*–*E* loop. Meanwhile, the ferroelectric polarization behavior was also tuned by the insertion of the HAO layer at different positions of the capacitor due to the change in the texture of the BCZT layer. The high linearity of hysteresis loops with low energy dissipation was achieved by placing the HAO layer between the BCZT and the top Au electrode. For the Pt/BCZT/HAO/Au capacitor, the obtained storage density and efficiency are 99.8 J cm^{-3} and 71.0%, respectively. Moreover, the energy storage performance of the present capacitors was stable up to 10^8 cycles. The resistive switching effect confirmed the presence of the charge coupling at the interface and thus modified the energy storage properties accordingly. Therefore, the present work showed that the integration of ferroelectric with dielectric layers may be an effective way to improve the energy storage performance of dielectric capacitors.

4. Experimental Section

By using a commercially available HfO_2:Al_2O_3 = 1:1 (Goodfellow, 99.9%) target and a BCZT target prepared by conventional solid state reaction as previously described by Silva et al.,[37] the BCZT/HAO, HAO/BCZT and BCZT/HAO/BCZT multilayered thin films were grown, by ion beam sputter deposition (IBSD) technique on top of Si/SiO_2/TiO_2/Pt substrates. The system was equipped with a multitarget carousel that allowed deposition of both layers successively, without breaking the vacuum. The vacuum chamber was first evacuated down to a low pressure of 1×10^{-6} mbar prior to the deposition. During the deposition, the substrate was kept at a temperature of 330 °C and at a distance of 87.3 mm from the target. The gas pressure inside the chamber was maintained constant at 2.5×10^{-4} mbar. A gas flow of 6.0 mL min^{-1} of Ar + 2.0 mL min^{-1} of O_2 was introduced into the ion beam gun and the atoms were ionized in the ion source with an rf-power of 120 W. The ions beam was further accelerated at 900 V and the ion beam current was regulated to remain at 31 mA. To grow the BCZT/HAO bilayers, first a BCZT layer with thickness of 150 nm was deposited on a Pt/TiO_2/SiO_2/Si substrate. Next, a 10 nm thick HAO layer was grown and, after the deposition, the bilayers were annealed in air at 750 °C. Similarly, HAO (10 nm)/BCZT (150 nm) bilayered and BCZT (75 nm)/HAO

Table 3. Comparison of the energy storage density and efficiency obtained in this work with the ones presented in the literature for ferroelectric and ferroelectric–dielectric based capacitors.

Materials	Film thickness [nm]	Fabrication method	E [kV cm^{-1}]	W_{rev} [J cm^{-3}]	η(%)	Ref.
BCZT	360	PLD	2080	39.11	33	[14]
$Pb(Zr_{0.52}Ti_{0.48})O_3$	300	PLD	1000	9.2	56.4	[30]
$0.94(Bi_{0.5})TiO_3$–$0.06BaTiO_3$/$BiFeO_3$	400	Sol–gel	2400	31.96	61	[4]
Mn-doped $0.7(Na_{0.5}Bi_{0.5})TiO_3$–$0.3SrTiO_3$	190	Sol–gel	1894	27	<50	[31]
$Pb_{0.90}La_{0.10}(Zr_{0.52}Ti_{0.48})O_3$	500	PLD	1500	23.2	91.6	[32]
$Ba(Zr_{0.2}Ti_{0.8})O_3$	350	Magnetron sputtering	5700	166	80	[33]
$Na_{0.5}K_{0.5}NbO_3$–$BiMnO_3$	700	Sol–gel	800	14.8	79	[34]
$0.25BiFeO_3$–$0.75BaTiO_3$	180	PLD	2050	52.2	–	[24]
$BiFeO_3$/$Bi_{3.25}La_{0.75}Ti_3O_{12}$/$BiFeO_3$	320	CSD	2753	65.5	74.2	[8]
$0.9(0.94(Na_{0.5}Bi_{0.5})TiO_3$–$0.06BaTiO_3)$–$0.1NaNbO_3$	300	Magnetron sputtering	3170	32	90	[35]
$Ba_{0.7}Ca_{0.3}TiO_3$/$BaZr_{0.2}Ti_{0.8}O_3$	100	Magnetron sputtering	4500	52.4	72.3	[36]
$PbZr_{0.52}Ti_{0.48}O_3$/Al_2O_3/$PbZr_{0.52}Ti_{0.48}O_3$	330	Sol–gel	5500	63.7	81.3	[19]
$0.5Ba(Zr_{0.2}Ti_{0.8})O_3$–$0.5(Ba_{0.7}Ca_{0.3})TiO_3$/$HfO_2$:$Al_2O_3$	160	Ion-beam sputtering	750	99.8	71.0	This work

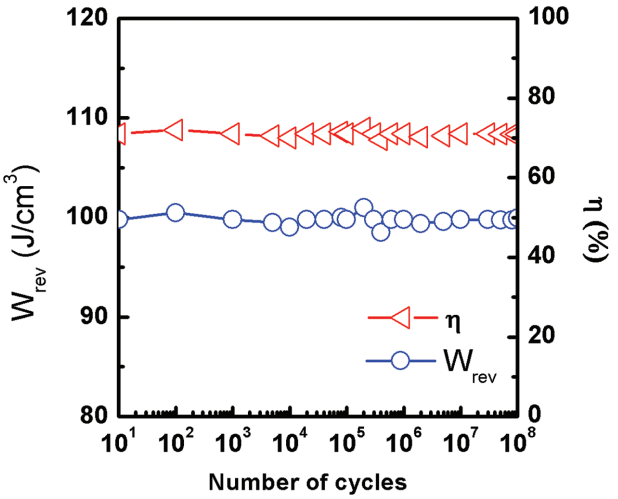

Figure 9. Energy density and efficiency as a function of the number of cycles for the Pt/BCZT/HAO/Au capacitors.

(10 nm)/BCZT (75 nm) trilayered thin films were grown on Pt/TiO_2/SiO_2/Si under identical conditions.

The thin films were structurally characterized by GIXRD with a Bruker D8 Discover diffractometer using Cu-Kα radiation (λ = 1.54056 Å) and an incident beam angle of 1.5°. AES analyses were performed with a "Physical Electronics PHI 710e/680 Hybrid" field emission scanning Auger microscope (SAM). Acceleration voltage of the exciting electron beam was fixed at 10 keV, and the sample current was aligned to 10 nA. The AES depth profiles were obtained by using a 2 keV Ar ion beam. The sputtering rate was 4 nm min^{-1} for a SiO_2 standard. After the profiles, the elemental maps were measured at the crater edge. For the ferroelectric and electrical characterization, circular gold (Au) electrodes having a diameter of 1 mm were deposited by thermal evaporation on the upper surface of the structure. The ferroelectric hysteresis loops (*P–E*) were measured at room temperature, with a modified Sawyer-Tower circuit using a sinusoidal signal at 1 kHz, while the dielectric response was measured using an Agilent E4980A LCR meter in the frequency range of 100 Hz to 1 MHz with an AC measuring voltage of 50 mV. The *I–V* characteristics were measured using a Keithley 617 programmable electrometer. The fatigue test was done by using the same modified Sawyer-Tower circuit at 100 kHz.

Acknowledgements

This work was supported by: i) the Portuguese Foundation for Science and Technology (FCT) in the framework of the Strategic Funding Contract UID/FIS/04650/2013 and ii) the Project Norte-070124-FEDER-000070 Nanomateriais Multifuncionais. Part of this work was carried out with the support of the Karlsruhe Nano Micro Facility (KNMF), a Helmholtz Research Infrastructure at Karlsruhe Institute of Technology (KIT), under the proposal 2017-017-017030. J.P.B.S. is grateful for financial support through the FCT Grant No. SFRH/BPD/92896/2013. K.C.S. acknowledges UGC and DST-SERB, Govt. of India for the funds through Grant Nos. F.4-5(59-FRP/2014(BSR)) and ECR/2017/000068, respectively. The authors would also like to thank Engineer José Santos for the technical support at the Thin Films Laboratory (Univ. Minho).

Conflict of Interest

The authors declare no conflict of interest.

Keywords

charge coupling effect, dielectric capacitors, energy efficiency, energy storage density, ferroelectric–dielectric structures

[1] S. Siddiqui, D.-I. Kim, L. T. Duy, M. T. Nguyen, S. Muhammad, W.-S. Yoon, N.-E. Lee, *Nano Energy* **2015**, *15*, 177.
[2] Y. Hao, X. Wang, K. Bi, J. Zhang, Y. Huang, L. Wu, P. Zhao, K. Xu, M. Lei, L. Li, *Nano Energy* **2017**, *31*, 49.
[3] Z. Pan, L. Yao, J. Zhai, K. Yang, B. Shen, H. Wang, *ACS Sustainable Chem. Eng.* **2017**, *5*, 4707.
[4] P. Chen, S. Wu, P. Li, J. Zhai, B. Shen, *Inorg. Chem. Front.* **2018**, *5*, 2300.
[5] H. Palneedi, M. Peddigari, G.-T. Hwang, D.-Y. Jeong, J. Ryu, *Adv. Funct. Mater.* **2018**, *28*, 1803665.
[6] Z. Tang, J. Ge, H. Ni, B. Lu, X.-G. Tang, S.-G. Lu, M. Tang, J. Gao, *J. Alloys Compd.* **2018**, *757*, 169.
[7] B. Peng, Z. Xie, Z. Yue, L. Li, *Appl. Phys. Lett.* **2014**, *105*, 052904.
[8] K. Yao, S. Chen, M. Rahimabady, M. S. Mirshekarloo, S. Yu, F. E. H. Tay, T. Sritharan, L. Lu, *IEEE Trans. Ultrason. Ferroelectr. Freq. Control* **2013**, *58*, 1968.
[9] B. B. Yang, M. Y. Guo, L. H. Jin, X. W. Tang, R. H. Wei, L. Hu, J. Yang, W. H. Song, J. M. Dai, X. J. Lou, X. B. Zhu, Y. P. Sun, *Appl. Phys. Lett.* **2018**, *112*, 033904.
[10] D. K. Kwon, M. H. Lee, *IEEE Trans. Ultrason. Ferroelectr. Freq. Control* **2012**, *59*, 1894.
[11] M. McMillen, A. M. Douglas, T. M. Correia, P. M. Weaver, M. G. Cain, J. M. Gregg, *Appl. Phys. Lett.* **2012**, *101*, 242909.
[12] T. Zhang, W. Li, Y. Zhao, Y. Yu, W. Fei, *Adv. Funct. Mater.* **2018**, *28*, 1706211.
[13] V. S. Puli, D. K. Pradhan, D. B. Chrisey, M. Tomozawa, G. L. Sharma, J. F. Scott, R. S. Katiyar, *J. Mater. Sci.* **2013**, *48*, 2151.
[14] V. S. Puli, D. K. Pradhan, S. Adireddy, R. Martínez, P. Silwal, J. F. Scott, C. V. Ramana, D. B. Chrisey, R. S. Katiyar, *J. Phys. D: Appl. Phys.* **2015**, *48*, 355502.
[15] J. P. B. Silva, K. Kamakshi, R. F. Negrea, C. Ghica, J. Wang, G. Koster, G. Rijnders, F. Figueiras, M. Pereira, M. J. M. Gomes, *Appl. Phys. Lett.* **2018**, *113*, 082903.
[16] D. Zhan, Q. Xu, D.-P. Huang, H.-X. Liu, W. Chen, F. Zhang, *J. Alloys Compd.* **2016**, *682*, 594.
[17] Q. Chi, T. Ma, Y. Zhang, Y. Cui, C. Zhang, J. Lin, X. Wang, Q. Lei, *J. Mater. Chem. A* **2017**, *5*, 16757.
[18] B. Peng, Q. Zhang, X. Li, T. Sun, H. Fan, S. Ke, M. Ye, Y. Wang, W. Lu, H. Niu, J. F. Scott, X. Zeng, H. Huang, *Adv. Electron. Mater.* **2015**, *1*, 1500052.
[19] J. P. B. Silva, K. Kamakshi, K. C. Sekhar, E. C. Queiros, J. A. Moreira, A. Almeida, M. Pereira, P. B. Tavares, M. J. M. Gomes, *J. Phys. D: Appl. Phys.* **2016**, *49*, 335301.
[20] J. P. B. Silva, F. L. Faita, K. Kamakshi, K. C. Sekhar, J. A. Moreira, A. Almeida, M. Pereira, A. A. Pasa, M. J. M. Gomes, *Sci. Rep.* **2017**, *7*, 46350.
[21] S. Mueller, J. Mueller, A. Singh, S. Riedel, J. Sundqvist, U. Schroeder, T. Mikolajick, *Adv. Funct. Mater.* **2012**, *22*, 2412.
[22] M. Mai, B. Martin, H. Kliem, *J. Appl. Phys.* **2011**, *110*, 064101.
[23] Y. D. Kolekar, A. Bhaumik, P. A. Shaikh, C. V. Ramana, K. Ghosh, *J. Appl. Phys.* **2014**, *115*, 154102.
[24] Z.-M. Wang, K. Zhao, X.-L. Guo, W. Sun, H.-L. Jiang, X.-Q. Han, X.-T. Tao, Z.-X. Cheng, H.-Y. Zhao, H. Kimura, G.-L. Yuan, J. Yinh, Z.-G. Liuh, *J. Mater. Chem. C* **2013**, *1*, 522.

[25] L. Pintilie, in *Ferroelectrics – Physical Effects*, (Ed.: M. Lallart), InTech, Rijeka, **2011**, pp. 101–134.
[26] J. M. B. Silva, J. P. B. Silva, K. C. Sekhar, M. Pereira, M. J. M. Gomes, *Appl. Phys. Lett.* **2018**, *113*, 102904.
[27] S. R. Reddy, V. V. B. Prasad, S. Bysakh, V. Shanker, J. Joardar, S. K. Roy, *J. Am. Ceram. Soc.* **2018**, https://doi.org/10.1111/jace.15983.
[28] N. D. Scarisoreanu, F. Craciun, A. Moldovan, V. Ion, R. Birjega, C. Ghica, R. F. Negrea, M. Dinescu, *ACS Appl. Mater. Interfaces* **2015**, *7*, 23984.
[29] S. Cho, C. Yun, Y. S. Kim, H. Wang, J. Jian, W. Zhang, J. Huang, X. Wang, H. Wang, J. L. MacManus-Driscoll, *Nano Energy* **2018**, *45*, 398.
[30] M. D. Nguyen, E. P. Houwman, M. Dekkers, C. T. Q. Nguyen, H. N. Vu, G. Rijnders, *APL Mater.* **2016**, *4*, 80701.
[31] Y. Zhang, W. Li, W. Cao, Y. Feng, Y. Qiao, T. Zhang, W. Fei, *Appl. Phys. Lett.* **2017**, *110*, 243901.
[32] M. D. Nguyen, C. T. Q. Nguyen, H. N. Vu, G. Rijnders, *J. Eur. Ceram. Soc.* **2018**, *38*, 95.
[33] H. Cheng, J. Ouyang, Y.-X. Zhang, D. Ascienzo, Y. Li, Y.-Y. Zhao, Y. Ren, *Nat. Commun.* **2017**, *8*, 1999.
[34] S. Yizhu, Z. Yunpeng, L. Qingshan, Z. Shifeng, *Phys. Status Solidi RRL* **2018**, *12*, 1700364.
[35] Y. Yao, Y. Li, N. Sun, J. Du, X. Li, L. Zhang, Q. Zhang, X. Hao, *J. Alloys Compd.* **2018**, *750*, 228.
[36] Z. Sun, C. Ma, M. Liu, J. Cui, L. Lu, J. Lu, X. Lou, L. Jin, H. Wang, C.-L. Jia, *Adv. Mater.* **2016**, *29*, 1604427.
[37] J. P. B. Silva, E. C. Queirós, P. B. Tavares, K. C. Sekhar, K. Kamakshi, J. Agostinho Moreira, A. Almeida, M. Pereira, M. J. M. Gomes, *J. Electroceram.* **2015**, *35*, 135.